Modern Mechanical Engineering, 2026, 16(4), 140-158
https://www.scirp.org/journal/mme
ISSN Online: 2164-0181
ISSN Print: 2164-0165

A Rapid Static Assessment Method for a UR121 Upright-Piano Soundboard Based on Finite-Element Calibration and Discrete Bridge-Load Redistribution

Wei Xiao[1], Wei Su[2*], Chengzhong Gong[1]

[1]Guangzhou Pearl River Kayserburg Piano Co., Ltd., Guangzhou, China
[2]School of Aeronautics and Astronautics, Sun Yat-sen University, Shenzhen, China
Email: *suwei@mail.sysu.edu.cn

How to cite this paper: Xiao, W., Su, W. and Gong, C.Z. (2026) A Rapid Static Assessment Method for a UR121 Upright-Piano Soundboard Based on Finite-Element Calibration and Discrete Bridge-Load Redistribution. *Modern Mechanical Engineering*, **16**, 140-158.
https://doi.org/10.4236/mme.2026.164008

Received: August 14, 2026
Accepted: September 26, 2026
Published: September 29, 2026

Abstract

For a fixed upright-piano geometry, repeating a complete three-dimensional finite-element (FE) analysis for every design adjustment is demanding, yet a single global empirical formula gives little insight into how the load is shared by individual ribs. To address this practical gap, a hierarchical rapid static-assessment method is developed for preliminary screening of the UR121 soundboard. Using the FE baseline to set the reported response scale, 438 discrete string-downbearing forces are distributed among 11 ribs by a normalized, load-conserving rule, from which rib-wise deflection, bending moment, and end reactions are obtained. Candidate changes in rib number and orientation can also be examined without altering the total applied load. A three-level 15/10/5 mm mesh assessment is reported; global deformation differs by no more than 4.5900% from the fine level, while local principal-stress extrema remain mesh-sensitive.

Keywords

Piano Soundboard, Static Response, Finite-Element Calibration, Reduced-Order Model, Load Transfer, Parametric Analysis

1. Introduction

Static downbearing from the complete string set reaches the piano soundboard through the bridges and is then carried by the thin wooden panel, the ribs, and the bonded perimeter. The resulting preloaded condition is relevant not only to deformation and connection stresses but also to the integrity of the assembly and its later vibroacoustic behaviour. Because the soundboard has an irregular outline, curved bridge paths, discrete load locations, and ribs of unequal geometry, its load path cannot be described adequately by one plate or beam expression.

Modal experiments and interferometric measurements have revealed the strongly spatial character of piano-soundboard vibration; these observations also provide an experimental basis for finite-element representations [1]-[3].

Related finite-element work has considered manufacturing stages, string down-bearing, prestress, and the influence of ribs, bridges, and material orientation [4]-[8]. Its emphasis, however, has generally remained on modal or vibroacoustic behaviour, usually through comparatively detailed numerical models.

What remains less developed for a fixed upright-piano system is a rapid static procedure that brings together FE response anchoring, normalized, load-conserving allocation of hundreds of discrete bridge loads, global equivalent stiffness, and finite rib-wise beam responses. The present work is directed at this narrower engineering requirement.

Accordingly, the proposed tool is positioned between a single empirical formula and a complete three-dimensional FE analysis. The work establishes the UR121 FE response scale, assigns 438 load points to 11 finite ribs through a normalized, load-conserving rule, and calculates rib-wise deflection, bending moment, and reactions. It also examines local variations in rib width, rib height, and equivalent modulus. Rib number and orientation are retained as candidate parameters, with geometry and load mapping regenerated automatically whenever either parameter is changed.

2. Methods

2.1. Hierarchical Framework

The calculation proceeds through a one-way hierarchy. At the first level, the three-dimensional FE model defines the response-scale baseline; the second level uses global equivalent stiffness to describe the overall response; and the third retains the individual bridge-load points, finite rib segments, and rib-wise mechanical indicators. An offline HTML/JavaScript application implements the rapid model and exports the derived CSV files programmatically. As shown in **Figure 1**, the framework proceeds from the three-dimensional FE baseline, through normalized allocation of the 438 discrete loads, to rib-wise beam indicators. This one-way chain uses the FE results to set the reported response scale; the reduced model does not feed back to modify the FE solution, and new geometries remain screening cases that require FE checking.

2.2. Three-Dimensional Finite-Element Baseline

A linear static solution of the baseline model was obtained in ANSYS Workbench. The wood assembly used $E_{\mathrm{FE}} = 14.15\ \mathrm{GPa}$ and $\nu = 0.328$. These homogeneous, isotropic, linear-elastic constants define a common static reference basis for the reported UR121 model; they do not assert physical isotropy of wood. The formal response anchor used a nominal 10 mm mesh and fully constrained the peripheral bonding region in all three translational directions.

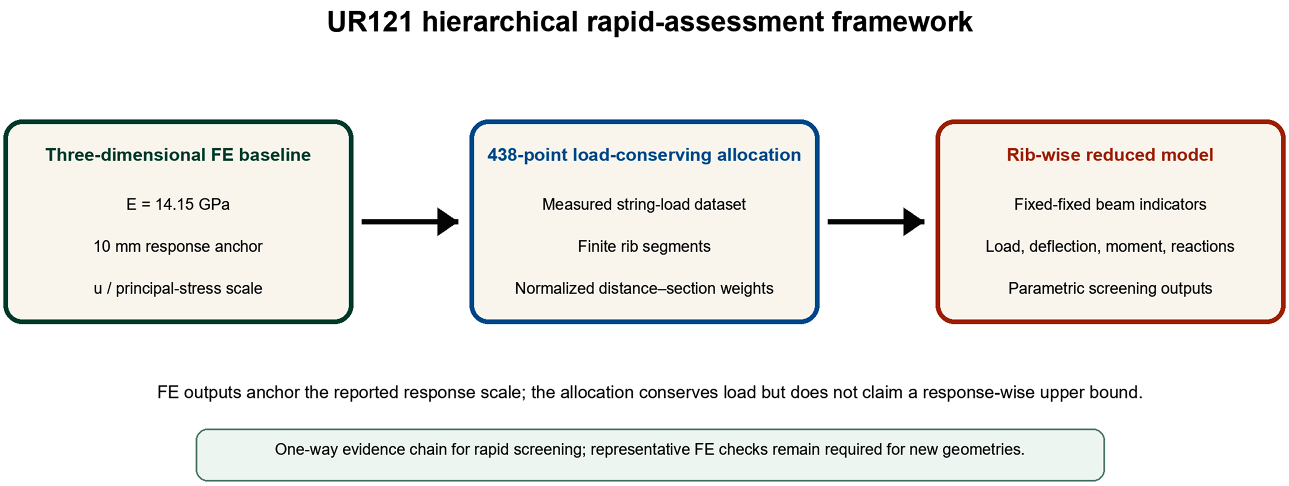

Figure 1. Hierarchical rapid-assessment method and one-way evidence chain.

Load-field definition and direction. The UR121 load chain comprised 88 notes and 219 physical strings (14 single-, 17 double-, and 57 triple-string notes). Two bridge-contact records were assigned to each string, yielding 438 source points. String tension was calculated as $T = 4\mu l^2 f^2$, where μ, l, and f denote mass per unit length, speaking length, and frequency, respectively. The two bridge-normal components were evaluated separately as $\frac{TH}{L_1}$ and $\frac{Th}{L_2}$ from the measured bearing-geometry ratios. Only the global Z component was retained because the analysis isolated static downbearing normal to the modeled soundboard; in-plane side-bearing forces, bridge axial/shear effects, and local force couples were outside the model scope. Accordingly, $F_x = F_y = 0$; positive tabulated Z-direction magnitudes denoted loads directed into the soundboard, and the opposite-sign global reaction was used as the equilibrium check. The individual values and their total satisfied $1.9377 \le F_z \le 20.3159\ \text{N}$ and $\sum_{i=1}^{438} F_{z,i} = 4234.2501\ \text{N}$, respectively.

Material-property basis and effective-isotropic representation. The available manufacturer test record identifies spruce specimens loaded parallel to grain and reports mean values of $E_{\text{FE}} = 14.15\ \text{GPa}$ and $\nu = 0.328$. No more specific species identification, moisture content, or conditioning information was available. These values were assigned uniformly to the soundboard, ribs, and bridges as effective scalar properties for the baseline static analysis. This representation provides a common stiffness scale for evaluating global deformation and load transfer and does not imply physical isotropy of wood. Because orthotropic and moisture-dependent behavior was not resolved, isolated local stress extrema were interpreted as localization indicators rather than verified material-strength limits. Application to a different wood stock or moisture condition requires replacement of the elastic inputs with properties measured for that condition.

Three-level mesh-sensitivity assessment. The same UR121 geometry, material basis, boundary conditions, 438-point load definition, and response measures were evaluated with nominal 15, 10, and 5 mm tetrahedral meshes containing 84,481/45,362, 164,516/89,904, and 648,965/373,536 nodes/solid elements, respectively. Mesh adequacy was judged mainly from maximum total deformation together with the spatial form of the displacement field. The three maximum values were 1.1488, 1.2168, and 1.1634 mm. Measured against the fine mesh, the coarse and baseline results differed by 1.2549% and 4.5900%, while the location of the high-deformation region and the overall bending pattern changed little. On that basis, the baseline mesh was used for the principal analyses, offering a practical balance between response stability and computational demand. The mesh data and response differences are summarized in Table 3.

Global coordinate convention. The global origin was fixed at the boundary point that appears at the upper left when the soundboard is viewed from the rib side. Figure 2 and Figure 3 show the bridge side; because the viewing direction is reversed, the same physical point appears at the upper right in these figures. In the rib-side view, the +X axis points to the right and the +Y axis points upward in the soundboard plane. Accordingly, in Figure 2 and Figure 3, the projection of the +X axis points to the left, whereas +Y remains upward. The +Z axis is normal to the soundboard plane and points from the bridge side toward the rib side. The panel occupies mainly positive X and negative Y, and all locations in Table 1 are reported in this fixed global coordinate system.

2.3. Geometry and Cross-Sections

The baseline geometry was reconstructed from the UR121 soundboard CAD/DXF drawing. Ribs 1-11 were numbered from left to right, and each effective span was defined as the longest portion of the finite rib centreline lying inside the soundboard boundary. The width/height pairs used for ribs 1 - 11 were 22/17, 22/18, 23/19, 26/22, 28/24, 30/25, 30/25, 28/24, 24/21, 22/18, and 20/16 mm, respectively.

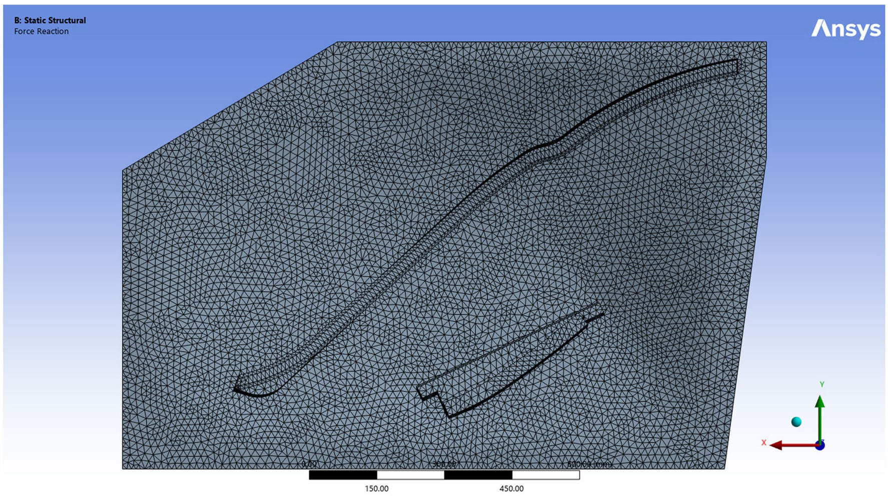

Figure 2. UR121 three-dimensional FE model and 10 mm mesh, bridge side.

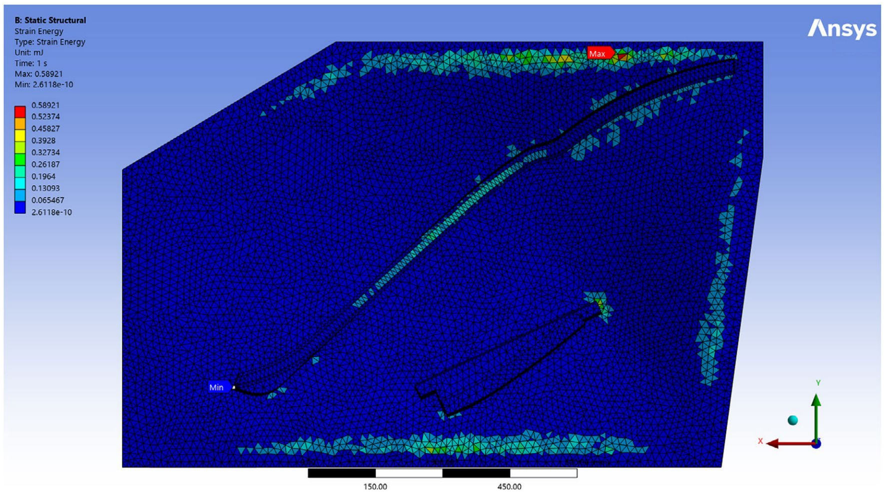

Figure 3. Strain-energy distribution for the 10 mm-mesh baseline, bridge side; maximum 0.5892 mJ.

Table 1. Key finite-element baseline responses and locations.

FE metric	Value	Unit/location
Maximum total deformation	1.2168	mm; approximately (583, −449, 8) mm
Maximum principal stress	10.3950	MPa; approximately (210, −230, 22) mm
Minimum principal stress	−20.8360	MPa; approximately (319, −26.9, 10.7) mm
Maximum equivalent stress	12.6600	MPa; approximately (321, −28.5, 10.7) mm
Minimum Z-directional displacement	−0.01297	mm; approximately (68.9, −37.1, −33.8) mm

2.4. Global Equivalent Stiffness and Discrete-Load Allocation

For a rectangular rib, the second moment of area follows the standard rectangular-section relation [9]:

$$I_j = \frac{b_j h_j^3}{12} \tag{1}$$

At the global screening level, the bending-stiffness contributions of the plate and ribs are combined into a relative indicator. The distance-section weighting rule is defined specifically for the present rapid model. For every load point i, the shortest distance d_{ij} to each finite rib segment j is evaluated, after which only the nearest $m = 3$ ribs are retained. The resulting unnormalized weight is

$$a_{ij} = \frac{I_j^{\alpha}}{\left(d_{ij} + d_0\right)^q} \tag{2}$$

In the current software implementation, $\alpha = 0.35$, $q = 2$, and $d_0 = 25$ mm are engineering-model parameters. Let i identify a load point, j identify a rib, and $\mathcal{N}_i$ denote the candidate-rib set associated with load point i. The normalized allocation coefficient and the load accumulated by rib j are then written as

$$W_{ij}=\frac{a_{ij}}{\sum_{k\in N_i}a_{ik}},P_j=\sum_{i=1}^{438}W_{ij}P_i \tag{3}$$

The normalization is applied separately to each load point, so that $\sum_{j\in N_i}W_{ij}=1$. Consequently, the global allocation satisfies $\sum_{j=1}^{11}P_j=\sum_{i=1}^{438}P_i$. The parameters α,q,d_0,m are empirical engineering-model settings rather than material constants or statistical confidence estimates. Here $P_i=F_{z,i}$, and $W_{ij}=0$ for $j\notin N_i$.

Because the allocation weights were normalized separately for each source point, the procedure preserved every applied point load and, consequently, the global total. Here, *load-conserving* refers only to this force-preservation property; it does not imply that rapid-model deformation or stress provides an upper bound on the corresponding FE response.

2.5. Finite Fixed-Fixed Beam Solution

Each rib is idealized as a fixed-fixed Euler-Bernoulli beam with length L_j [9]. The reduced model and FE baseline both use $E_{\text{eq}}=E_{\text{FE}}=14.15\ \text{GPa}$. Distinct symbols are retained to distinguish the equivalent modulus in the beam reduction from the modulus assigned to the three-dimensional FE assembly, although their numerical values are identical in the present study. Under multiple concentrated loads, the governing equation becomes

$$E_{\text{eq}}I_j\frac{\mathrm{d}^4w_j(x)}{\mathrm{d}x^4}=\sum_r P_{jr}\delta\left(x-x_{jr}\right) \tag{4}$$

Here r indexes the source-load contributions assigned to rib j; $P_{jr}=W_{rj}P_r$, and x_{jr} is the projected coordinate of source r along the finite rib segment. The implementation evaluates the signed beam solution under its internal moment convention and reports $\max_x\left|w_j(x)\right|$; this internal sign choice does not affect the magnitude indicators.

Downward load and downward deflection are taken as positive in the rapid-model magnitude convention. The fixed-end boundary conditions are $w_j(0)=w_j'(0)=w_j\left(L_j\right)=w_j'\left(L_j\right)=0$. Linear superposition of the concentrated-load solutions gives $w_j(x),M_j(x)$, and the end reactions [9]. A correction factor $c_b=0.55$ multiplies the raw beam-deflection indicator before baseline normalization; this factor is a fixed engineering-model parameter applied only to the intermediate beam-deflection indicator; it is not the direct multiplier from that indicator to the FE maximum deformation and is not applied to reaction, bending moment, or raw beam stress. The resulting rib-wise deflection and FE-anchored rib stress outputs remain relative indicators and are not direct wood-strength criteria. Using $\sigma=\frac{Mc}{I}$ for a rectangular section [9], the positive bending-stress indicator is

$$\sigma_{j,\text{ind}}=\frac{6M_{j,\max}}{b_jh_j^2} \tag{5}$$

In Equation (5), the moment term is the maximum absolute bending moment along the rib, and the width and height terms are the corresponding cross-section dimensions.

Fixed model parameters and FE-referenced response scaling. The reduced model uses $E_{\text{eq}} = E_{\text{FE}} = 14.15\ \text{GPa}$ together with the prescribed engineering parameters $c_b = 0.55$, $\alpha = 0.35$, $q = 2$, $d_0 = 25$ mm, $m = 3$, and $\alpha_p = 0.28$. These parameters define the reduced-order formulation and were not estimated by regression or multi-case FE optimization. Deformation and principal-stress indicators are normalized by their respective baseline reduced-model values and scaled by the corresponding 10 mm FE baseline responses. The normalized response ratio therefore equals unity at the baseline by definition; exact recovery of the FE reference at that state is not an independent validation result.

Deflection and stress mappings. Let $w_{b,\max}^{\text{raw}}$ denote the maximum rib-beam deflection indicator evaluated at the reference modulus $E_{\text{eq}}^{(0)}$, $w_{b,\max}$ denote the intermediate corrected indicator, and $w_{b,\max}^{(0)}$ denote its baseline value; $\lambda_E = \dfrac{E_{\text{eq}}}{E_{\text{eq}}^{(0)}}$ denotes the equivalent-modulus multiplier. The intermediate step is $w_{b,\max} = c_b w_{b,\max}^{\text{raw}}$. For the baseline configuration, $5.5973 \times 0.55 \approx 3.0785$ mm. The FE-referenced deformation mapping is $r_b = \dfrac{w_{b,\max}}{\lambda_E w_{b,\max}^{(0)}}$, $r_w = \alpha_p + (1 - \alpha_p) r_b$, and $w = 1.2168 r_w$ mm. At baseline, $\lambda_E = 1$, $r_b = \dfrac{3.0785}{1 \times 3.0785} = 1$, $r_w = \alpha_p + (1 - \alpha_p) \times 1 = 0.28 + 0.72 \times 1 = 1$, and $w = 1.2168$ mm. For stress, the largest rib-level indicator from Equation (5) is used in $r_\sigma = \dfrac{\sigma_{b,\max}}{\sigma_{b,\max}^{(0)}}$, $\sigma_t = 10.3950 r_\sigma$ MPa, and $\sigma_c = -20.8360 r_\sigma$ MPa. The subscripts identify beam, maximum, tension, and compression quantities, while the superscripts raw and (0) identify the unmultiplied and baseline states. These equations reproduce the FE baseline values by construction and do not establish validation away from the baseline.

As summarized in Table 2, the equivalent modulus is the common scalar modulus used by both models, whereas the deflection correction factor, plate-share coefficient, load-allocation exponent, distance offset, and nearest-rib settings are prescribed reduced-model parameters. The baseline-relation column also shows that exact reference recovery follows from normalization and that the allocation conserves total force without establishing a response bound.

2.6. Parametric Geometry and Load Redistribution

The actual baseline comprises 11 ribs and uses a common orientation parameter of 54˚. If rib number or orientation is altered, the previous load shares are discarded. New rib centrelines are generated, clipped to the actual soundboard boundary, and reduced to their longest internal segments; b and h are obtained by linear interpolation between adjacent baseline ribs. The software subsequently recalculates the distances from all 438 load points and redistributes the loads through Eqs. (2)-(3). Changes in rib number or orientation therefore modify the effective span, interpolated cross-section, load share, and beam response at the same time. As shown in Figure 4, the interface connects the parameter controls with the regenerated rib geometry and displays both the conserved load total and the FE-referenced assembly responses. The 3.0785 mm intermediate beam indicator is reported separately from the 1.2168 mm assembly deformation, consistent with the two-stage mapping defined above.

Table 2. Rapid-model parameters and FE baseline reference responses.

Quantity	Value	Function	Baseline relation	Parameter basis
Equivalent scalar modulus E_{eq}	14.15 GPa	Common scalar modulus for the FE and reduced-beam models	$E_{eq} = E_{FE}$	Common FE/reduced-model value
Beam multiplier c_b	0.55	Intermediate beam-deflection scaling before baseline normalization	Cancels from the same-setting baseline ratio	Prescribed model parameter
Plate-share coefficient α_p	0.28	Combines the invariant plate share with the beam-response ratio	Baseline $r_w = 1$ by construction	Prescribed model parameter
Allocation settings	$\alpha = 0.35$; $q = 2$; $d_0 = 25$ mm; $m = 3$	Normalized allocation to the nearest three ribs	Total load conserved to numerical roundoff; no response bound	Prescribed model parameters
FE response anchors	1.2168 mm; +10.3950/−20.8360 MPa	Scale deformation and principal-stress ratios	Normalized baseline ratio = 1 by definition	FE baseline response

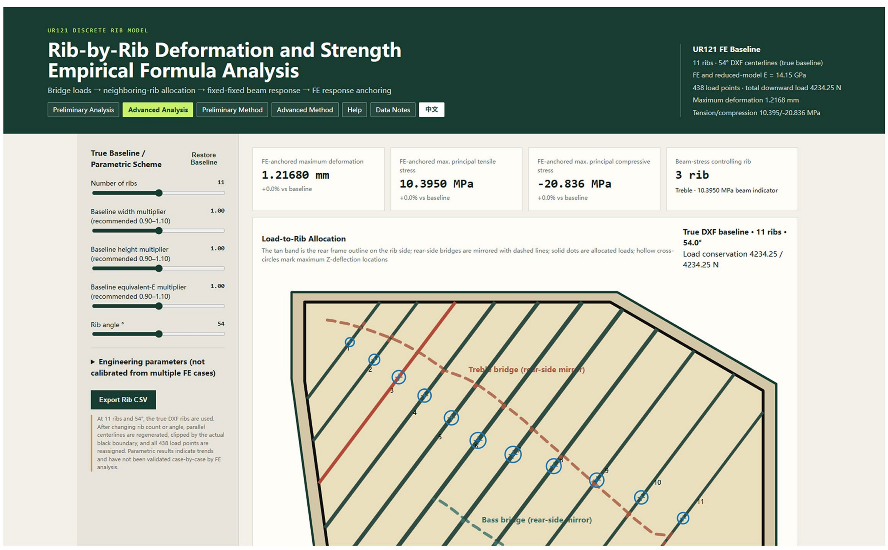

Figure 4. Software interface for the 11-rib, 54˚ UR121 baseline. The upper cards display FE-referenced assembly responses, while the soundboard schematic below shows the corresponding load redistribution. The 3.0785 mm value is obtained from $5.5973 \times 0.55 \approx 3.0785$ mm and is subsequently used in the baseline ratio normalization that gives the 1.2168 mm assembly-level response.

2.7. Cases and Numerical Verification

For the fixed geometry, rib width, rib height, and E_{eq} are each varied by ±10%. Separate parametric-geometry cases contain 9, 10, 12, or 13 ribs and use orientation angles of 48˚, 51˚, 57˚, or 60˚. Internal numerical checks cover conservation of the 438 loads, balance of rib reactions, stability with respect to beam-axis sampling, and reproduction of the baseline outputs. Existing strain measurements are used more narrowly for a semi-quantitative comparison of response magnitude, high-response regions, and spatial trends.

3. Results

3.1. FE Baseline and Numerical Checks

With the 10 mm mesh, the baseline reached a maximum total deformation of 1.2168 mm. Its maximum and minimum principal stresses were 10.3950 and −20.8360 MPa, and its maximum equivalent stress was 12.6600 MPa. Imported Force transferred all 438 source points, and the source and target totals were 4234.2501 N. The rapid model assigned the same 4234.2501 N in total, with the largest rib reaction-balance error below 6.3×10^{-13} N. Increasing the beam-axis sampling from 141 to 281 points raised the maximum beam indicator (3.0785 → 3.0787 mm), an increase of 0.0067%.

FE-referenced response scaling and mesh sensitivity. At the baseline reduced-model state, deformation and stress ratios are unity, so the reported outputs equal 1.2168 mm, +10.3950 MPa, and −20.8360 MPa. This equality follows from normalization and is not an independent prediction residual. Across the nominal 15/10/5 mm meshes, maximum total deformation was 1.1488/1.2168/1.1634 mm; relative to the 5 mm result, the 15 and 10 mm values differed by 1.2549% and 4.5900%, respectively. The location of the high-deformation region and the overall bending pattern changed little, supporting use of the 10 mm baseline as a practical balance between spatial resolution and computational demand. Maximum equivalent stress was 10.3850/12.6600/12.8940 MPa, with corresponding differences of 19.4587% and 1.8148%. Full results are reported in Table 3.

Table 3. Three-level FE mesh-sensitivity comparison.

Mesh level	Nominal size	Nodes/elements	Principal FE response measures
Coarse	15 mm	84,481 nodes; 45,362 solid elements	$u_{max} = 1.1488$ mm; $\sigma_{1,max} = 8.1598$ MPa; $\sigma_{3,min} = -15.6620$ MPa; $\sigma_{eq,max} = 10.3850$ MPa
Baseline	10 mm	164,516 nodes; 89,904 solid elements	$u_{max} = 1.2168$ mm; $\sigma_{1,max} = 10.3950$ MPa; $\sigma_{3,min} = -20.8360$ MPa; $\sigma_{eq,max} = 12.6600$ MPa
Fine	5 mm	648,965 nodes; 373,536 solid elements	$u_{max} = 1.1634$ mm; $\sigma_{1,max} = 17.0140$ MPa; $\sigma_{3,min} = -17.3380$ MPa; $\sigma_{eq,max} = 12.8940$ MPa

As shown in Figure 5 and Figure 6, the rib-side and bridge-side views produce the same 1.2168 mm maximum total deformation, with a broad high-deformation region in the central panel. Figure 7 shows that the negative principal-stress bands on the bridge side are concentrated along the bridges and adjacent boundary regions, whereas Figure 8 shows that the Z-directional deformation closely reproduces the total-deformation field, indicating that the static response is dominated by out-of-plane motion. Figure 9 and Figure 10 show the maximum-principal-stress fields from the rib and bridge sides; in both views, the 10.3950 MPa peak is localized near the upper boundary rather than at the central deformation maximum. Figure 11 shows that the rib-side compressive extrema are likewise confined to localized rib and perimeter regions, while Figure 12 shows higher equivalent stress along selected stiffeners and boundary regions. Figure 13 further shows localized strain-energy accumulation along particular ribs and adjacent boundary regions, consistent with nonuniform load transfer through the stiffened assembly.

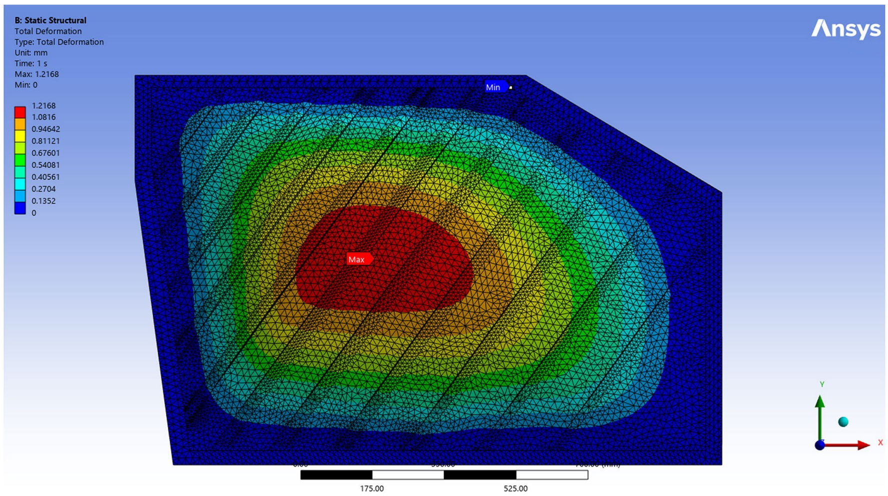

Figure 5. Total deformation for the 10 mm-mesh baseline, rib side; maximum 1.2168 mm.

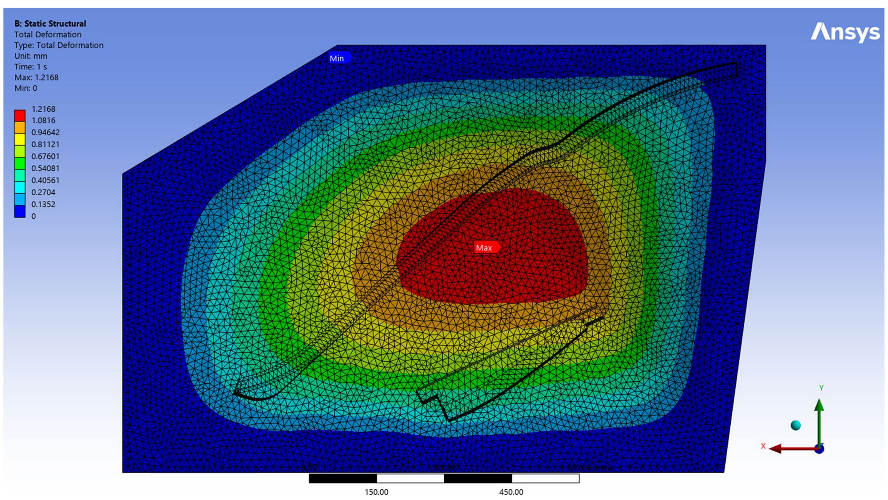

Figure 6. Total deformation for the 10 mm-mesh baseline, bridge side; maximum 1.2168 mm.

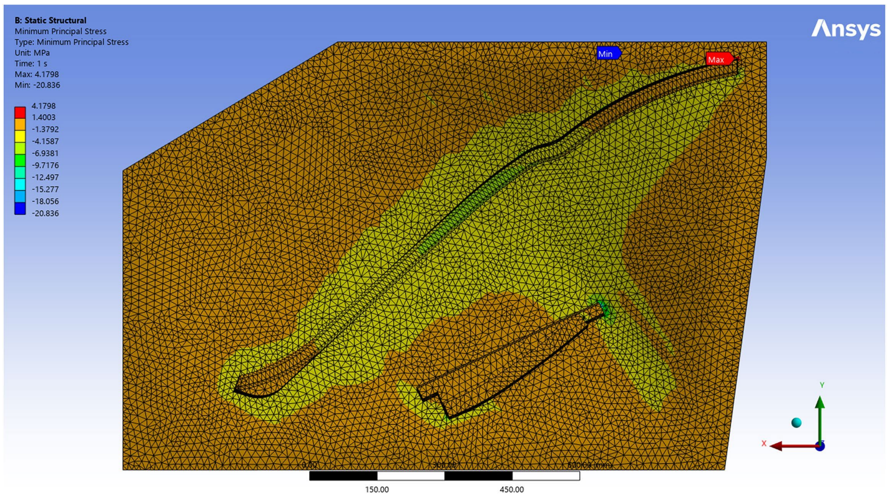

Figure 7. Minimum principal stress, bridge side; minimum −20.8360 MPa.

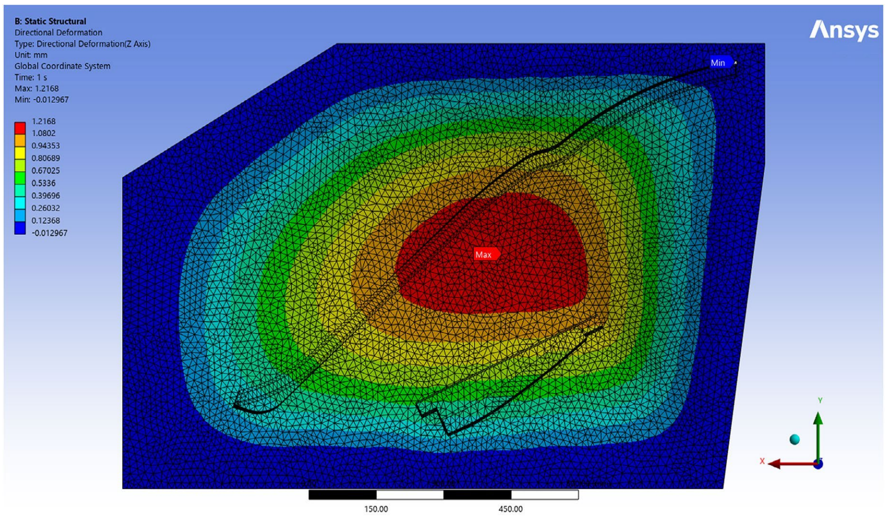

Figure 8. Z-directional deformation, bridge side; maximum 1.2168 mm.

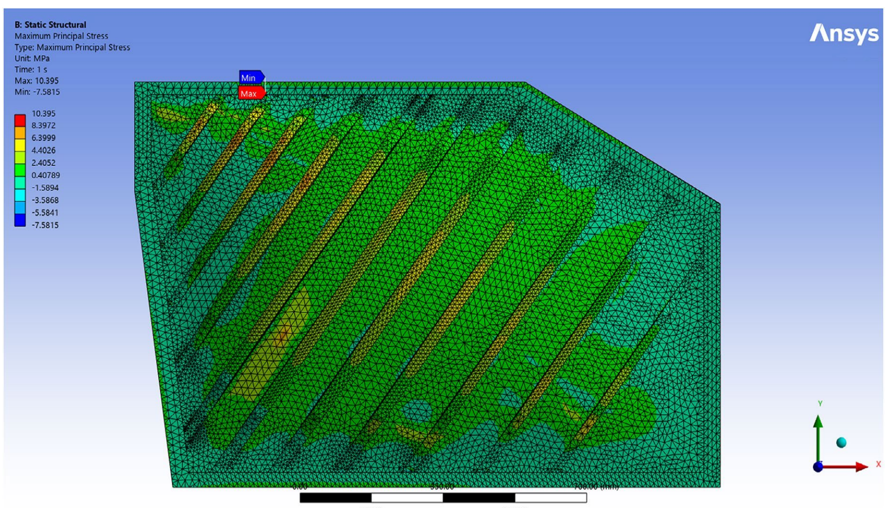

Figure 9. Maximum principal stress, rib side; maximum 10.3950 MPa.

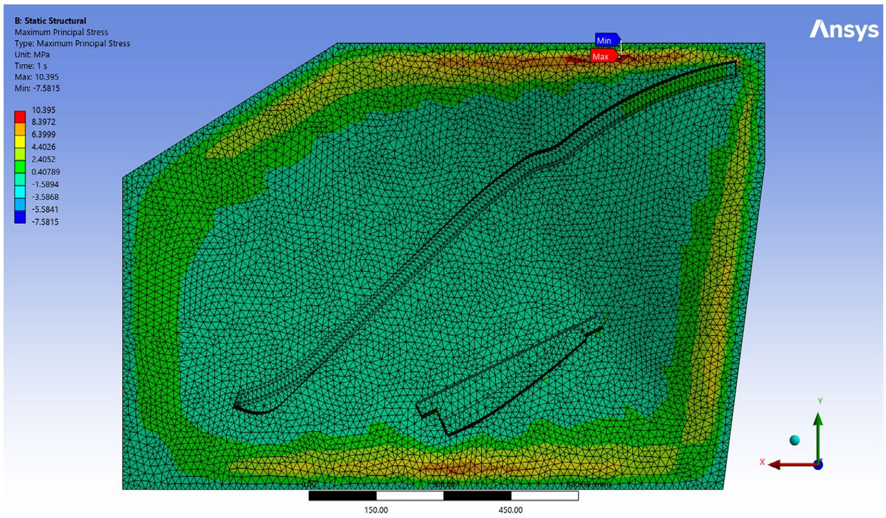

Figure 10. Maximum principal stress, bridge side; maximum 10.3950 MPa.

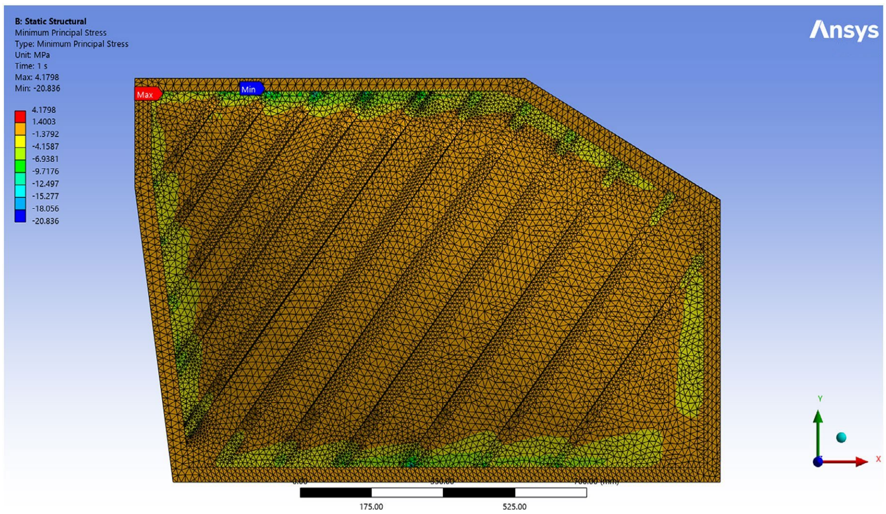

Figure 11. Minimum principal stress distribution on the rib side; minimum −20.8360 MPa.

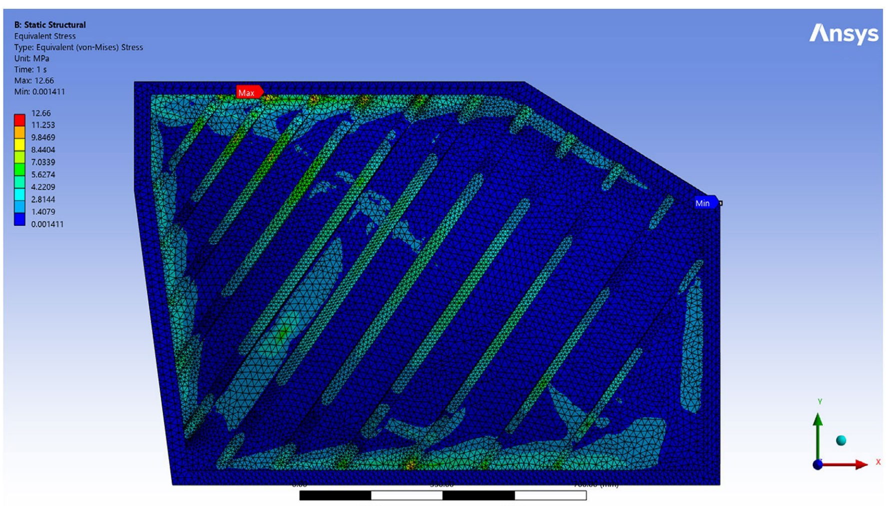

Figure 12. Equivalent (von Mises) stress distribution on the rib side; maximum 12.6600 MPa.

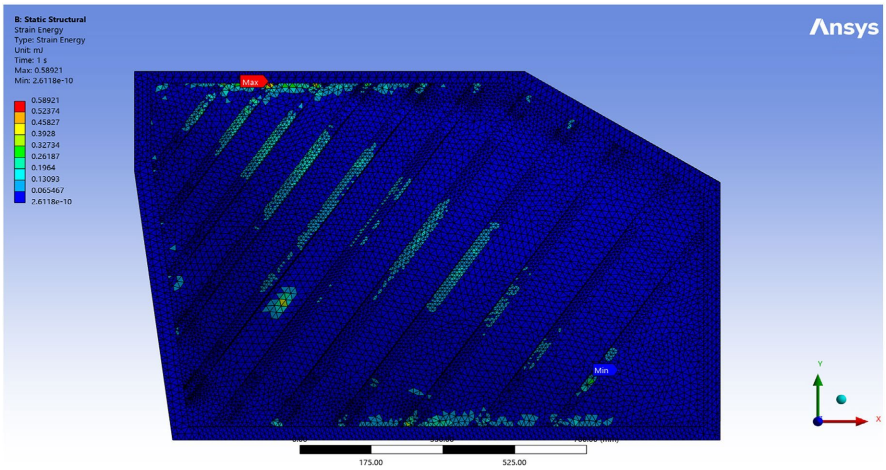

Figure 13. Strain-energy distribution on the rib side; maximum 0.5892 mJ.

3.2. Baseline Rib-Wise Response

For the baseline geometry, the largest load share was assigned to rib 7 (551.6850 N). The same rib also gave the highest intermediate beam-deflection indicator (3.0785 mm) and bending moment (78.3400 N·m). The FE-anchored rib stress indicator reached its maximum at rib 3, with a value of 10.3950 MPa; consequently, a single rib should not be assumed to govern every response measure. As shown in Figure 14, rib 7 simultaneously carries the largest allocated load and gives the largest intermediate beam-deflection and bending-moment indicators. The differing profiles across the other ribs show, however, that allocated load alone is not a complete proxy for rib-wise mechanical response.

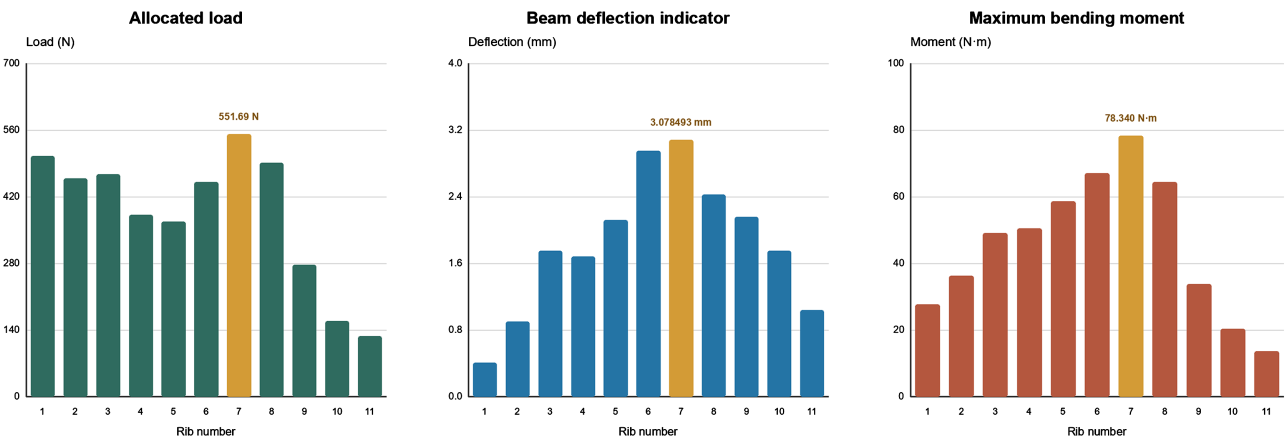

Figure 14. Allocated load, maximum intermediate beam-deflection indicator, and maximum bending moment for the 11 baseline ribs.

Mapped baseline deformation. The unmultiplied maximum rib-beam indicator is 5.5973 mm. Applying $c_b = 0.55$ once gives $5.5973 \times 0.55 \approx 3.0785$ mm, so the 3.0785 mm quantity is $w_{b,\max}$ rather than $w_{b,\max}^{\text{raw}}$. At the reference state, $\lambda_E = 1$, $r_b = \dfrac{3.0785}{1 \times 3.0785} = 1$, $r_w = \alpha_p + \left(1 - \alpha_p\right) \times 1 = 0.28 + 0.72 \times 1 = 1$, and $w = 1.2168$ mm. Thus, 3.0785 mm is an intermediate beam indicator rather than a direct prediction of assembly-level maximum deformation.

Mapped baseline stress. At the baseline, the normalized beam-stress ratio is unity, giving FE-referenced tensile and compressive indicators of +10.3950 and −20.8360 MPa, respectively. These are scaled response indicators rather than independent wood-strength predictions or validation residuals.

3.3. Local Sensitivity for Fixed Geometry

Relative to the 1.2168 mm baseline, a −10% change in every rib width increased the maximum deformation to 1.3141 mm, whereas a +10% change reduced it to 1.1372 mm. The same ordered pair was obtained for uniform −10% and +10% changes in E_{eq}, respectively. A −10% change in every rib height increased the response to 1.5425 mm, whereas a +10% change reduced it to 0.9989 mm. The beam contribution follows $w_b \propto (EI)^{-1}$ with $I \propto bh^3$, while the reported deformation retains the invariant plate share $\alpha_p = 0.28$. Because every rib was scaled by the same factor, $I^{0.35}$ cancels during normalization of the load allocation. The comparison therefore describes stiffness scaling rather than redistribution caused by modifying one rib alone.

Sensitivity relations. For uniform changes in E_{eq} or rib width,

$w_{-10\%} = 1.2168\left(0.28 + \dfrac{0.72}{0.9}\right) = 1.3141$ mm and

$w_{+10\%} = 1.2168\left(0.28 + \dfrac{0.72}{1.1}\right) = 1.1372$ mm. For uniform rib-height changes,

$w_{-10\%} = 1.2168\left[0.28 + \dfrac{0.72}{(0.9)^3}\right] = 1.5425$ mm and

$w_{+10\%} = 1.2168\left[0.28 + \dfrac{0.72}{(1.1)^3}\right] = 0.9989$ mm. In each pair, the first relation represents the −10% case and the second represents the +10% case. Figure 15 shows that rib-height variation produces the steepest change in normalized deformation, whereas the rib-width and equivalent-modulus curves coincide. This reflects the cubic dependence on rib height and the linear dependence on width and modulus in the reduced beam-stiffness relation.

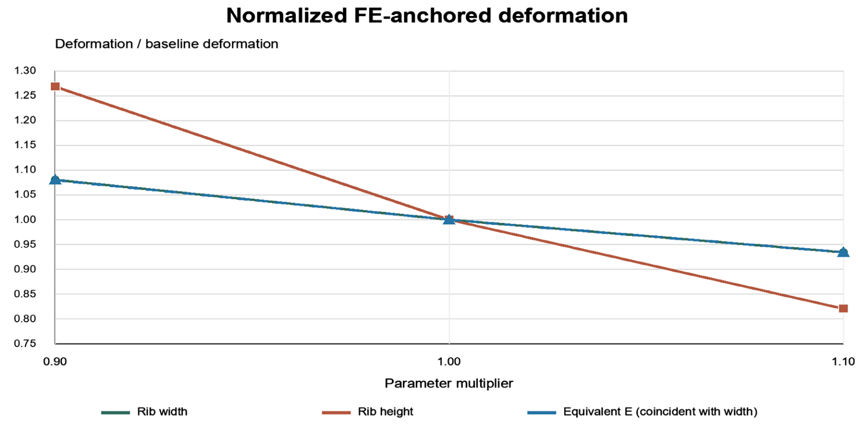

Figure 15. Normalized maximum deformation for ±10% changes in rib width, rib height, and equivalent modulus.

3.4. Candidate Rib-Number and Angle Cases

Every candidate rib-number and orientation case retained all 438 load points and the total load of 4234.2501 N. With 9 rather than 11 ribs, the maximum deformation rose to 1.5426 mm and the tensile principal stress to 13.6581 MPa. The 13-rib case gave lower values of 1.1526 mm and 10.2890 MPa. Orientation produced a similar contrast in deformation: changing 54˚ to 48˚ increased the maximum to 1.3797 mm, whereas 60˚ reduced it to 1.1010 mm. The tensile-stress indicator varied much less with orientation. These outputs should be read as the combined outcome of span clipping, cross-section interpolation, and load redistribution.

Common response mapping. All candidate deformations in this section use the same normalized beam ratio and $\alpha_p = 0.28$ plate-share mapping, and all reported principal-stress values use the same baseline stress-ratio anchors. The candidate geometries were not evaluated using independent three-dimensional FE simulations and are therefore interpreted as screening indicators.

As summarized in Table 4 and plotted in Figure 16, increasing rib count from 9 to 13 generally reduces both maximum deformation and principal tensile stress, although the 12-rib tensile response is slightly above the 11-rib baseline. Increasing the common rib angle from 48˚ to 60˚ reduces deformation monotonically, while the tensile-stress indicator remains close to the baseline.

Figure 17 shows the regenerated 13-rib geometry and redistributed load field; the interface retains the full 4234.2501 N load and reports lower deformation and principal-stress magnitudes than the 11-rib baseline. Figure 18 shows the regenerated 60˚ geometry; the altered spans and load shares reduce maximum deformation to 1.1010 mm while slightly increasing the tensile and compressive principal-stress magnitudes relative to the baseline.

Table 4. Candidate responses for changes in rib number and angle.

Case	n	Angle (deg)	Maximum deformation (mm)	Principal tension (MPa)	Principal compression (MPa)
Baseline	11	54	1.2168	10.3950	−20.8360
Rib count −2	9	54	1.5426	13.6581	−27.3766
Rib count −1	10	54	1.3317	12.1495	−24.3528
Rib count +1	12	54	1.1950	10.7201	−21.4876
Rib count +2	13	54	1.1526	10.2890	−20.6235
Angle −6 deg	11	48	1.3797	10.3975	−20.8409
Angle −3 deg	11	51	1.2925	10.3869	−20.8198
Angle +3 deg	11	57	1.1508	10.4569	−20.9601
Angle +6 deg	11	60	1.1010	10.5714	−21.1896

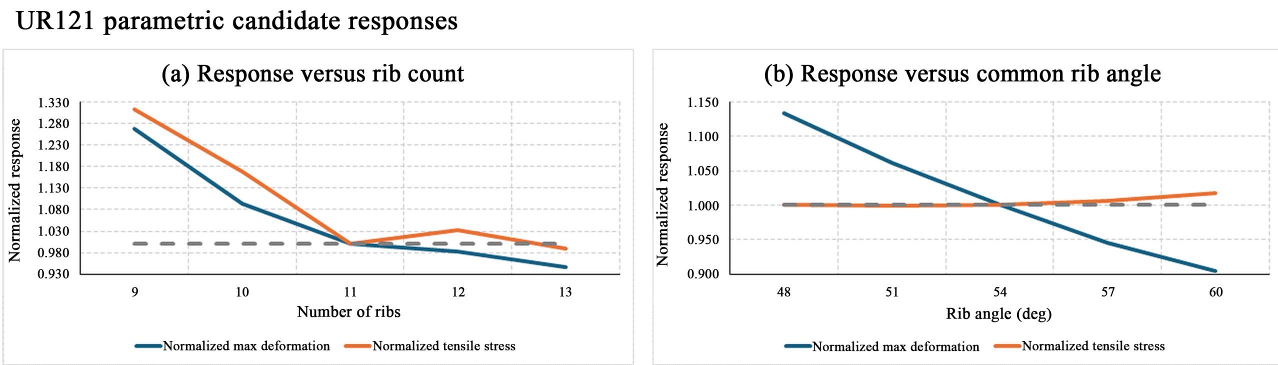

Figure 16. Candidate responses to changes in rib number and angle.

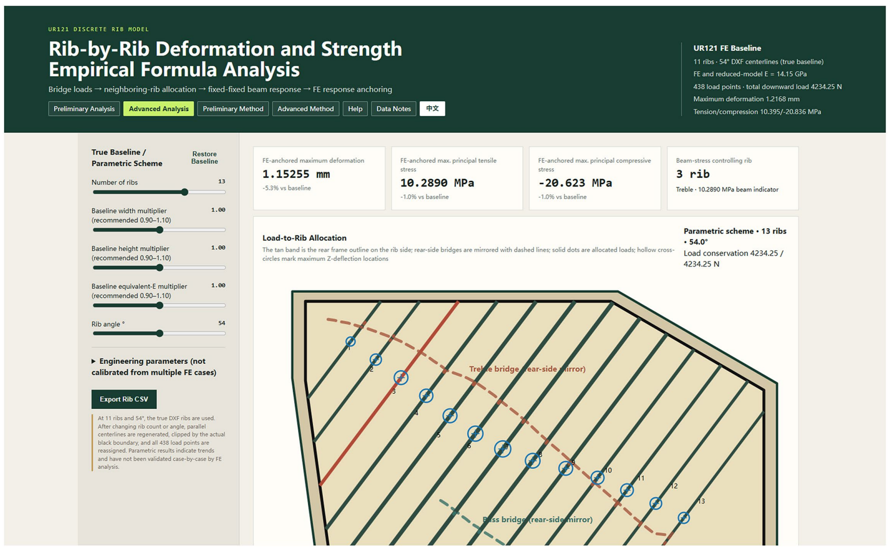

Figure 17. English software interface for the 13-rib parametric geometry, load allocation, and response.

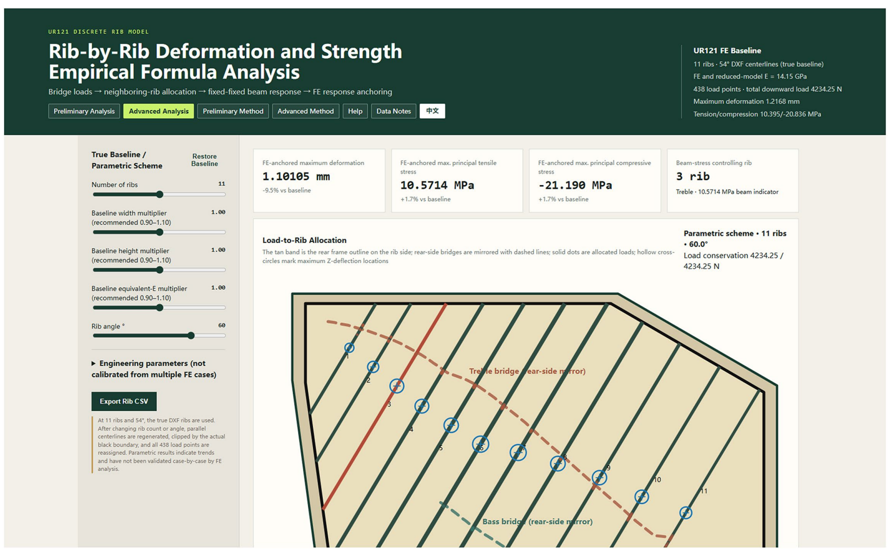

Figure 18. English software interface for the 60˚ parametric geometry, load allocation, and response.

4. Discussion

Three distinct evidence levels are connected in the proposed framework. The three-dimensional FE model sets the response scale for the UR121, the normalized, load-conserving allocation retains the discrete nature of the bridge loads, and the rib-wise beam model exposes how load, span, cross-section, and response are related. This gives more structural detail than a single global empirical formula while avoiding a new three-dimensional FE solution for every screening case. Even so, faster calculation and exact internal conservation do not by themselves demonstrate predictive accuracy outside the anchored baseline setting.

The fixed-geometry cases are consistent with the expected beam-stiffness scaling: width and modulus enter EI approximately linearly, while height acts through h^3. More ribs generally lead to a smaller maximum deformation, although the tensile stress in the 12-rib case is slightly higher than in the 11-rib baseline. This departure from a simple monotonic picture indicates that boundary clipping and redistribution can still govern a local response. Orientation has a clearer influence on deformation than on the present tensile-stress indicator. None of these trends should be separated from the particular UR121 parametric-generation rule used here.

The strength of each conclusion depends on the supporting evidence. Load conservation, reaction balance, beam-axis sampling stability, and reproduction of the baseline outputs show that the numerical implementation is internally consistent. The FE solution supplies the baseline response reference, whereas the strain measurements support only a semi-quantitative comparison of magnitude and high-response regions. Independent three-dimensional FE simulations were not performed for the candidate rib-number and orientation cases. Those cases are therefore screening results rather than fully validated designs, and they do not establish an optimum or transferability to other piano types.

Several modelling choices limit the interpretation of the results. The FE model uses an effective-isotropic material representation, while explicit orthotropy, moisture effects, adhesive layers, manufacturing residual stresses, and boundary rotational flexibility are omitted. The ribs are reduced to fixed-fixed Euler-Bernoulli beams. The three-level mesh study shows limited sensitivity of global displacement but strong sensitivity of isolated principal-stress extrema; those extrema are therefore not treated as mesh-independent strength values. The method is intended for relative comparisons within the fixed UR121 outline and present load locations, with emphasis on global deformation and continuous response patterns.

Material-condition dependence. Application beyond the reported UR121 material basis requires equivalent properties appropriate to the wood stock, grain direction, moisture content, and conditioning state of the soundboard being assessed.

5. Conclusions

1) The UR121 rapid static-assessment method combines an FE baseline with

global equivalent stiffness, normalized, load-conserving discrete-load allocation, and finite rib-beam responses.

2) The calculation retained all 438 bridge-load points, conserved 4234.2501 N, and limited the rib reaction-balance error to numerical-roundoff level.

3) In the actual baseline model, rib 7 governed the beam-deflection and bending-moment indicators, whereas rib 3 governed the reported stress indicator; the controlling rib therefore depends on the response measure considered.

4) Under uniform ±10% changes, rib height affected maximum deformation more strongly than either rib width or E_{eq}, consistent with rectangular-beam bending-stiffness scaling.

5) After a change in rib number or orientation, the software regenerates the geometry, clips the boundaries, interpolates the sections, and reallocates all 438 loads. The resulting cases are suitable for preliminary screening, although representative FE analyses are still required before their quantitative accuracy can be established.

Acknowledgements

The authors thank Yihua Li and Zhenhao Shi for their contributions to model development and experimental work.

Author Contributions

Conceptualization, Wei Xiao and Chengzhong Gong; methodology, Wei Su. All authors have read and agreed to the published version of the manuscript.

Conflicts of Interest

The authors declare no conflicts of interest regarding the publication of this paper.

References

[1] Berthaut, J., Ichchou, M.N. and Jézéquel, L. (2003) Piano Soundboard: Structural Behavior, Numerical and Experimental Study in the Modal Range. *Applied Acoustics*, **64**, 1113-1136. https://doi.org/10.1016/s0003-682x(03)00065-3

[2] Chaigne, A., Cotté, B. and Viggiano, R. (2013) Dynamical Properties of Piano Soundboards. *The Journal of the Acoustical Society of America*, **133**, 2456-2466. https://doi.org/10.1121/1.4794387

[3] Moore, T.R. and Zietlow, S.A. (2006) Interferometric Studies of a Piano Soundboard. *The Journal of the Acoustical Society of America*, **119**, 1783-1793. https://doi.org/10.1121/1.2164989

[4] Corradi, R., Fazioli, P., Miccoli, S. and Squicciarini, G. (2011) Modal Analysis and Finite Element Modelling of a Grand Piano Soundboard. *Proceedings of the* 8*th International Conference on Structural Dynamics*, *EURODYN* 2011, Leuven, 4-6 July 2011, 3176-3183.

[5] Corradi, R., Miccoli, S., Squicciarini, G. and Fazioli, P. (2017) Modal Analysis of a Grand Piano Soundboard at Successive Manufacturing Stages. *Applied Acoustics*, **125**, 113-127. https://doi.org/10.1016/j.apacoust.2017.04.010

[6] Mamou-Mani, A., Frelat, J. and Besnainou, C. (2008) Numerical Simulation of a Pi-

ano Soundboard under Downbearing. *The Journal of the Acoustical Society of America*, **123**, 2401-2406. https://doi.org/10.1121/1.2836787

[7] Mamou-Mani, A., Le Moyne, S., Ollivier, F., Besnainou, C. and Frelat, J. (2012) Prestress Effects on the Eigenfrequencies of the Soundboards: Experimental Results on a Simplified String Instrument. *The Journal of the Acoustical Society of America*, **131**, 872-877. https://doi.org/10.1121/1.3651232

[8] Mokdad, F. and Missoum, S. (2013) A Fully Parameterized Finite Element Model of a Grand Piano Soundboard for Sensitivity Analysis of the Dynamic Behavior. *ASME* 2013 *International Design Engineering Technical Conferences and Computers and Information in Engineering Conference*, Portland, 4-7 August 2013, USA, DETC2013-13193, V008T13A072. https://doi.org/10.1115/detc2013-13193

[9] Young, W.C. and Budynas, R.G. (2002) Roark's Formulas for Stress and Strain. 7th Edition, McGraw-Hill.